Preprint typeset using LaTeX style emulateapj v. 12/16/11

EVALUATION OF A TECHNIQUE TO DIFFERENTIATE AXION SIGNALS FROM RADIO-FREQUENCY INTERFERENCE SIGNALS IN ADMX

Michaela Guzzetti [1], Gray Rybka[2]

(Dated: August 31, 2019)

ABSTRACT

For years astronomers and physicists have observed the effects of dark matter, but to this day its true nature remains, more or less, a mystery. As astronomers ruled out existing astrophysical bodies, physicists began looking to the Standard Model for answers. The strongly favored cold dark matter (CDM) particle candidate for many years was the WIMP. In recent years, however, the popularity of the axion has been on the rise and groups like the Axion Dark Matter eXperiment (ADMX) collaboration are using axion haloscopes to listen for this form of invisible dark matter. This paper outlines a method for differentiating axion-like signals from interference signals by utilizing chi-squared statistics and probability.

1. BACKGROUND

1.1. *Axion Theory and the Strong CP Problem*

Axions are light ($m_a \approx 1$ - 100 μeV) [1] pseudo-Goldstone bosons created as a consequence of the Peccei-Quinn (PQ) solution to the strong CP problem. That is to say, there exists a term in the QCD Lagrangian (equation 1) that violates P and T reversal symmetry, but conserves charge conjugation symmetry, thus violating CP symmetry via the CPT theorem.

$$L_\theta = \theta \frac{g^2}{32\pi^2} F_a^{\mu\nu} \tilde{F}_{a\mu\nu} \tag{1}$$

This in and of itself is not a problem. The problem arises from the fact that physicists expect to see a large neutron electric dipole moment (nEDM) as a result of this violation, but it has yet to be observed. This would insinuate that the CP violating term must somehow be essentially cancelled out. This requires an unnaturally small value of θ, particularly $\mathcal{O}(10^{-10})$ [2]. The resolution to this so-called 'fine-tuning problem' was offered via the PQ solution. This solution introduces a new global symmetry and makes θ a dynamic field, as opposed to a parameter which, in order to match measured values of the nEDM, requires fine-tuning to very high precision. The θ field's potential is represented by a the shape of the bottom of a wine bottle (Figure 1), with infinite equivalent minima. Spontaneous symmetry breaking in which one of the infinitely equivalent minima are 'chosen' at sufficiently low temperature produces massless Goldstone bosons under normal circumstances. However, if there is a small explicit symmetry breaking in addition to the spontaneous symmetry breaking which causes the potential to 'tip', singling out one of the infinite minima as the true minimum, the previously massless Goldstone boson acquires a mass. This process occurs for the $(1)_{PQ}$ symmetry and thus creates the pseudo-Goldstone boson of interest for this paper, the axion [3].

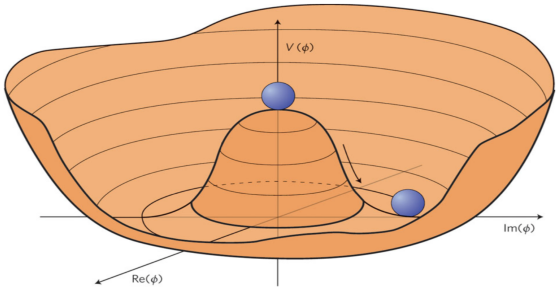

Fig. 1.— Wine Bottle potential with spontaneously broken U(1) symmetry (Brubaker 2018)

1.2. *Axions as CDM*

Axions, although originally theorized as a solution to the strong CP problem, soon became intriguing dark matter candidates for a few reasons. Before delving into why axions *do* make favorable CDM candidates it's pedagogically beneficial to briefly discuss why other particles do *not*.

Neutrinos are light, electrically neutral, weakly interacting, and stable. In almost every respect they seem like sound dark matter candidates. Neutrinos, however, are 'hot', meaning their speeds were still relativistic at the time galactic masses came within the horizon volume. Hot dark matter (HDM) would result in 'top-down' structure formation where galaxy clusters form first, and subsequently fragment into galaxies [4]. This structural evolution would cause our universe to differ greatly from what we observe today, which aligns more closely with 'bottom-up' structure formation; galaxies formed first, and later joined to form galaxy clusters. In addition to neutrinos being HDM as opposed to CDM, they are extremely light, meaning there would need to be an exceedingly large amount crammed into say, the Milky Way, in order to account for the known local dark matter density. So many in fact, that it would be impossible to fit them all. This is because neutrinos are, unfortunately, fermions. Due to the Pauli-exclusion principle, if we were to squish them all into our galaxy, for example, the fastest moving neutrinos would have a Fermi velocity greater than the escape velocity of the Milky Way [4]!

[1] Smith College Department of Physics & Astronomy, University of Washington INT REU Program
[2] University of Washington, Center for Experimental Nuclear Physics and Astrophysics

Another long-favored CDM candidate is the WIMP, or Weakly Interacting Massive Particle. Theoretically, WIMPs make good dark matter candidates and overall seem like they could be what physicists have been looking for. The only downside is, they haven't found them yet. Searches for WIMPs have been going on for quite sometime and many are becoming disillusioned with the hope of finding them. This isn't to say, of course, that WIMPs do not exist. It has just encouraged physicists to start looking in new directions, which brings us to the axion.

The axion checks many of the boxes neutrinos failed to. Because they are produced via the PQ or misalignment mechanism as opposed to being thermal relics of the Big Bang, axions are born cold and stay cold throughout their lifetimes. In addition to this, axions are bosons, meaning they don't have into the same issue neutrinos did with the Pauli-exclusion principle despite being extremely low mass. Not only do axions *not* have the problems neutrinos did, they have other promising pieces of evidence behind them as well. QCD numerical and analytical studies indicate the most likely axion mass to be in the μeV range. This is encouraging because axions are stable on cosmological timescales for $m_a \leq 26$ eV, and axions in the μeV range would coincide with an axion density which is comparable to that of dark matter ($\Omega_a = \Omega_{DM}$).

2. SEARCHING FOR THE AXION WITH ADMX

2.1. *Axion-Photon Conversion*

The Axion Dark Matter eXperiment (ADMX), led by Dr. Leslie Rosenberg, has called the Center for Experimental Nuclear Physics and Astrophysics (CENPA) at the University of Washington its home since 2010. Despite the experiment's physical location at UW, the ADMX collaboration is represented across multiple universities and organizations throughout the world. The experimental setup is characterized primarily by the use of an axion haloscope, which was first proposed by Pierre Sikivie in 1983 at the University of Florida. Axions will decay into two photons in a vacuum on their own, however they have extremely low decay rates so it was long thought they could not be detected [5], hence the term "invisible" often being used to describe dark matter axions (Figure 2, left). Fortunately, however, Maxwell's equations in the presence of axions are slightly altered, allowing the framework for axion haloscopes to exist.

$$\nabla \times \vec{B} = \frac{\partial \vec{E}}{\partial t} + \vec{J} - g_{a\gamma\gamma}(\vec{E} \times \nabla a - \frac{\partial \vec{a}}{\partial t}\vec{B}) \qquad (2)$$

$$\nabla \cdot \vec{E} = \rho - g_{a\gamma\gamma}\vec{B} \cdot \nabla a \qquad (3)$$

Equation 3, despite being affected by axions in theory, is not useful for the purpose of detecting dark matter axions as we assume the spatial distribution of dark matter axions to be practically uniform, thus the ∇a term goes to zero. Unlike equation 3, equation 2 is of particular interest to those searching for "invisible" axions since the axion field is oscillating with respect to time. It thus shows that the axion can interact with a magnetic field to produce a detectable current, $\vec{J}_a$. This can also be described via the Inverse Primakoff Effect, which is a variation of axion decay in a static magnetic field (Figure 2, right). In this process the static magnetic field can be visualized as a sea of virtual, zero momentum, photons. One of the previous two photons from vacuum axion decay is 'replaced' by one of these virtual photons, while the other has energy equal to the rest-mass energy of the axion, $m_a c^2$ plus the non-relativistic kinetic energy.

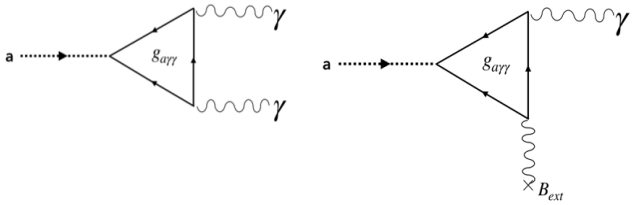

FIG. 2.— Diagram of the Primakoff Effect (left) and the Inverse Primakoff Effect (right). (Nicole Man)

2.2. *Axion Haloscopes*

Axion haloscopes take advantage of the Inverse Primakoff Effect to detect what were once considered impossible-to-detect dark matter axions. The haloscope ADMX uses is a cylindrical, copper-plated, resonant microwave cavity which is embedded inside a superconducting solenoid which produces a homogeneous magnetic field of 7.6 T (Figure 3).

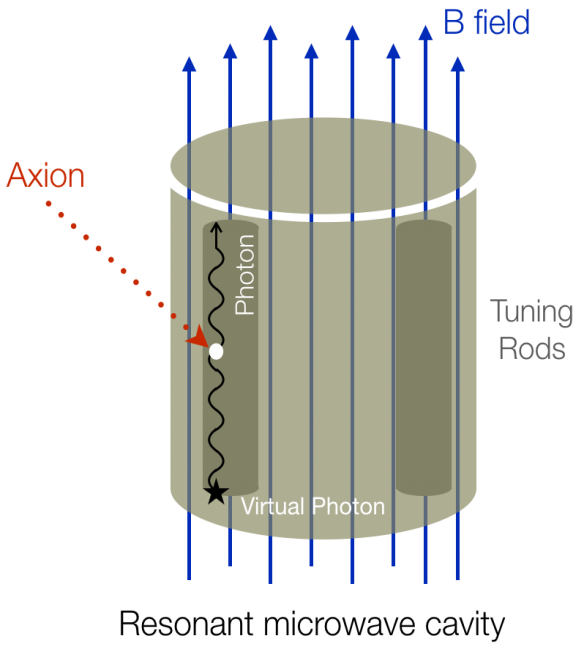

FIG. 3.— Diagram detailing the process of axion-photon conversion in an axion haloscope.

The experiment is designed to cover a frequency range that corresponds to the aforementioned μeV axion mass range. The cavity is tunable via two cylindrical tuning rods which can move from the walls to the center of the cavity, altering its geometry and thus its resonant frequency. This is of great importance since the exact ax-

ion mass is unknown, and the power of an axion signal is strongly correlated with how close the cavity resonance is to its frequency. This dependence is described by a Lorentzian (equation 4).

$$P(\Delta f) = P_{axion}\left(\frac{1}{1+4Q^2(\frac{\Delta f}{f})}\right) \tag{4}$$

Where P_{axion} is the expected on resonance axion power which depends on the cavity volume, the magnetic field strength, the form factor (a measure of the alignment of the external magnetic field and the axion's electric field), the model-dependent axion-photon coupling constant, the local dark matter density, the frequency of the cavity, and the cavity's quality factor. Figure 4 provides a visual representation of this dependence, also referred to as the cavity lineshape.

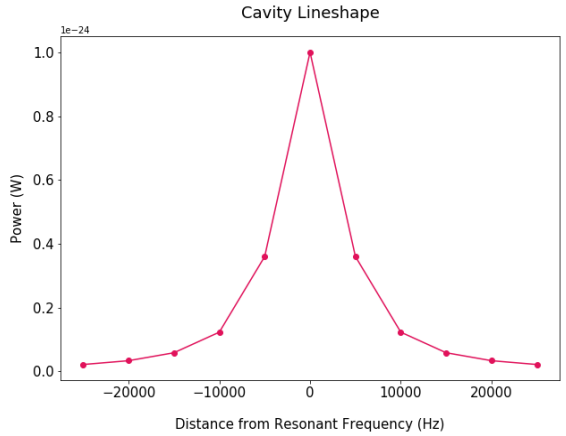

FIG. 4.— Power of a theoretical axion-like signal at different offsets from the cavity frequency. As the signal frequency drifts from the cavity resonant frequency, the power drops dramatically.

2.3. *Radio Frequency Interference Signals vs. Axion Signals*

In addition to in-cavity axion-like signals, there are instances of radio-frequency interference (RFI) signals. These RFI signals enter the detectors somewhere downstream in the electronics, instead of through the cavity as an axion-like signal would. Since these signals do not enter the cavity, they do not follow the cavity lineshape. Instead, their signal power is more or less constant over a range of cavity offsets, since they are not dependent on resonance. In other words, if an RFI signal were to be plotted on the same plot as Figure 4 it would roughly be a horizontal line. However, given a signal sampled at a single cavity frequency (one point on a plot like Figure 4), it is impossible to determine whether or not the signal is coming from inside or outside the cavity.

3. DIFFERENTIATING AXION-LIKE SIGNALS FROM RFI-LIKE SIGNALS

3.1. *My Model*

Currently, ADMX re-scans any power signal that is above a specificed power threshold. This could be caused by either an axion-like signal or an RFI-like signal, and with only one cavity frequency value it's impossible to distinguish the two from one another. In an attempt to streamline this process and avoid re-scanning so many RFI signals, I aimed to use fits and chi squared statistics to determine if a given signal is more likely to be axion-like or RFI-like.

To verify that this method is viable statistically, it needed to be tested on controlled, simulated data. For a simple, toy model, the simulated data consisted of signals that either followed the cavity lineshape or were constant with respect to frequency offset, both with Gaussian Johnson-Nyquist (thermal) noise for the cavity (equation 5) added in.

$$P_{noise} = k_B T\sqrt{\frac{b}{t}} \tag{5}$$

The normal distribution is centered on zero (since we are measuring power excess) and has a standard deviation represented by the equation 5. Where T, the temperature of the cavity, is 100 mK, b, the bandwidth of the measurement, is 100 Hz, and t, the time elapsed during the measurement, is 100s. Examples of these simulated signals can be seen in Figure 5.

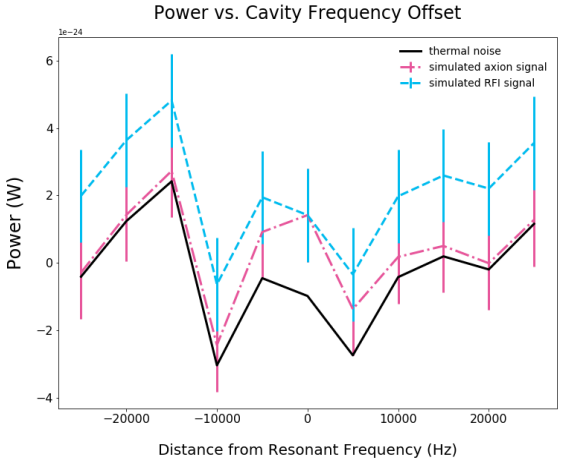

FIG. 5.— Example of a simulated axion signal and a simulated RFI signal against the thermal noise distribution with a signal-to-noise-ratio (SNR) of 3.

Figure 5 demonstrates that even with multiple cavity offsets, it is difficult to tell which one of the signals is following the cavity line shape due to the low SNR. This is where using chi-squared statistics can become useful as it allows us to compare how well two different functions fit a given signal better than we can by eye.

I will now outline the process for fitting and categorizing a given signal. For this simple model, it is assumed that a given signal either fits the cavity lineshape, or does not. It also assumes that I have a signal sampled at several cavity frequency offsets from the signal frequency. This is crucial because, as mentioned previously, axion-like and RFI-like signals are essentially indistinguishable when sampled at a single cavity frequency.

Once the data is simulated, it goes through a procedure to categorize it as either RFI-like or axion-like. This begins by fitting a given scan (a group of signal powers at different frequency offsets like those plotted

in Figure 5), with both the axion/Lorentzian fit, and the RFI/constant fit. Then, a chi-squared value is calculated for each fit with the simulated data. Finally, the chi squared values are subtracted from one another $\chi^2_{axion} - \chi^2_{RFI}$. This difference value, χ^2_{diff}, is used to categorize a signal as either RFI-like or axion-like. For example, if the axion fit was better it would have a smaller value of χ^2_{axion} than it would for χ^2_{RFI}, leading to a smaller, or possibly more negative value of χ^2_{diff}. However, if the RFI fit was better, the opposite would be true, leading to a larger, or more positive value of χ^2_{diff}. This categorization method will be discussed in more detail in Sec 3.2.

3.2. *Results*

This model was tested using 20,000 scans each of axion and RFI signals for a total of 40,000 samples total, each covering a cavity frequency that is ±25kHz from the signal frequency, all with random Johnson-Nyquist noise as outlined in Sec 3.1. Figures 6 and 7 are two examples of the simulated data for a simulated axion signal with the two fits and a simulated RFI signal with the two fits respectively.

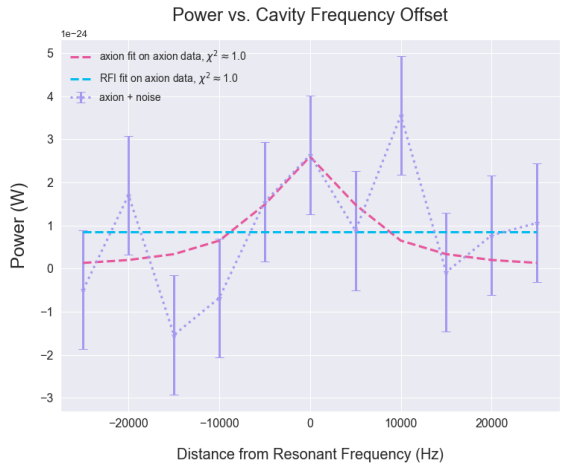

FIG. 6.— Simulated axion signal with a fit for the cavity lineshape (axion fit) and another for the out-of-cavity lineshape (RFI fit)

Figure 6 is an example of a case where, even using statistics, it is essentially impossible to distinguish whether or not the given signal is more likely to be axion or an RFI. This implies that there will be some region of overlap in the χ^2_{diff} distributions for axion signals and RFI signals due to the low SNR. Figure 7 shows however, that there are cases where statistics can fairly easily determine which fit is better.

Now that we have seen two individual examples, let's look at the χ^2_{diff} distributions for the full set of 20,000 scans (Figure 8). As mentioned in Sec 3.2. the simulated axion signals have a lower mean value for χ^2_{diff}, while the simulated RFI mean is greater. However, due to the low SNR there is an area of overlap, as expected. The goal of this process is to reduce the amount of RFI signals that are re-scanned, but ultimately ADMX's purpose is to find the axion. Therefore, above all, we want to preserve

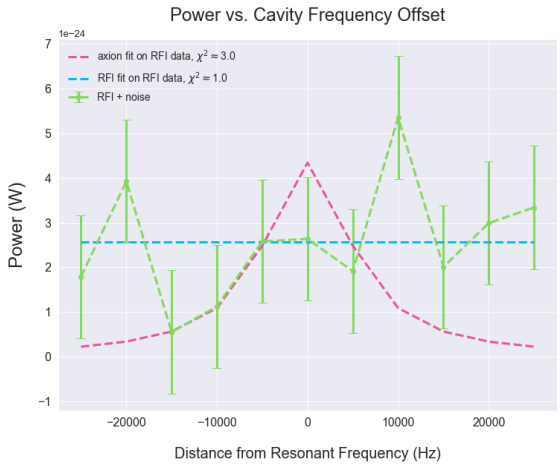

FIG. 7.— Simulated RFI signal with a fit for the cavity lineshape (axion fit) and another for the out-of-cavity lineshape (RFI fit)

axion signals.

To do this, the program determines a threshold value that will change depending on the SNR, but for an SNR of 3 is fairly consistently around 0.5. Any signal with a χ^2_{diff} below this threshold value will be categorized as axion-like (necessary to re-scan) and any signal with a χ^2_{diff} above this will be categorized as RFI-like (not considered for re-scanning). The threshold value changes with the SNR because the location of the overlap region changes, and as I mentioned previously we ultimately want to retain the axion signals. Thus, the threshold value will continuously increase, starting at some specified minimum value (for SNR =3, the minimum value is set as 0), in steps of +0.05 until 99% or greater of the axion signals are correctly identified, meaning we have a less than 1% chance of missing one if it were to enter the cavity. The effectiveness of this model can be seen best in Figure 9.

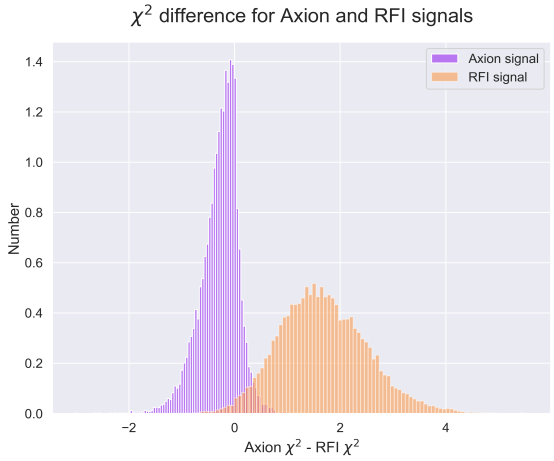

FIG. 8.— Distrubtion of χ^2_{diff} values for all 20,000 simulated axion signals and all 20,000 simulated RFI signals

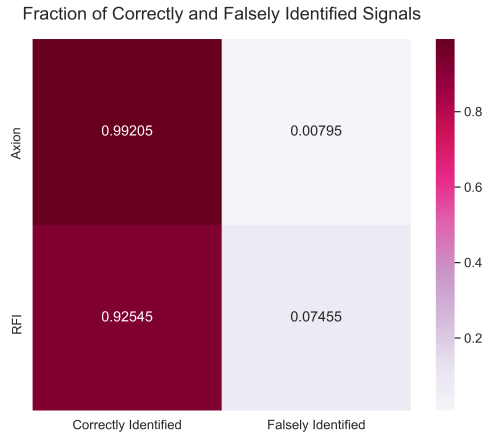

FIG. 9.— Fraction of simulated signals that were either correctly or falsely identified.

3.3. *Conclusions*

Through testing this model on a sample of 20,000 simulated axion and RFI signals respectively all with an SNR of 3, it can be seen that it is able to reject 93% of RFI signals, while still maintaining the utmost priority of correctly identifiying at least 99% of axion signals. This means we only need to re-scan 7% of signals that were previously being re-scanned. This would greatly reduce the amount of time it takes us to work through the theoretical mass range, meaning we will either find or exclude the axion sooner.

It is worth mentioning that for SNR lower than 3 the model still works but not quite as well. For an SNR of 2.2, for example, the amount of RFI signals that can be safely rejected (meaning we maintain that 99% or more of axion signals are found) drops from 93% to 73%. In addition to lowering the SNR, taking steps larger than 5kHz (less points total) reduces the effectiveness of the model. For example, if steps of 7kHz are taken to ±21kHz instead of steps of 5kHz to ±25kHz the amount of RFI signals that can be safely rejected drops to 78%. Lastly, if both of these conditions are true, only 50% of RFI signals can be safely rejected. Although these criteria cause the effectiveness to drop, this is still a huge improvement from before where all signals above the candidate threshold were re-scanned indiscriminately.

3.4. *Future Work*

The next step for this model is to test it on real data now that it has been proven to work on a toy model. This will be used to thoroughly check the validity of this method to ensure it can be trusted before implementing it in the greater analysis procedure.

4. ACKNOWLEDGEMENTS

I would like to thank everyone on the ADMX team at CENPA for their support and kindness this summer. I'd particularly like to thank the lead scientist of ADMX, Prof. Leslie Rosenberg and my advisor, Prof. Gray Rybka, for teaching me as much about axion physics as they could in 10 weeks and for being there to answer my questions along the way. I would also like to acknowledge the National Science Foundation for funding my research experience. The ADMX collaboration gratefully acknowledges support from the US Dept. of Energy, High Energy Physics DE-SC00116655 & DE-SC0010280 & DE-AC52-07A27344.

REFERENCES

[1]Du, N. et al. (ADMX Collaboration), Phys. Rev. Lett. 120, 151301 (2018). doi:10.1103/PhysRevLett.120.151301
[2]Sikivie, P., Physics Today 49, 12, 22 (1996). https://doi.org/10.1063/1.881573
[3]M. Tanabashi et al. (Particle Data Group), Phys. Rev. D 98, 030001 (2018).
[4]Brubaker, B. (2018). First results from the HAYSTAC axion search (Ph.D. Thesis). Retrieved from arXiv:1801.00835v1.
[5]Stern, I. (ADMX Collaboration),AIP Conf. Proc. 1604 (2014) 456-461. doi:10.1063/1.4883465